Electronic Supplementary Information for

Ni single atoms supported on hierarchically porous carbonized wood with highly active Ni-N$_4$ sites as a self-supported electrode for superior CO$_2$ electroreduction

Huaiyu Chang,[a,b] Hui Pan,[a] Fang Wang,[a] Zhengguo Zhang,[a] Yaming Kang[*b] and Shixiong Min[*a]

[a] School of Chemistry and Chemical Engineering, North Minzu University, Yinchuan, 750021, P. R. China.

[b] School of Electrical and Mechanical Engineering, North Minzu University, Yinchuan, 750021, P. R. China.

*Corresponding authors: sxmin@nun.edu.cn; scu.kym@foxmail.com

1. Experimental

1.1 Chemicals and materials

Basswood was purchased from Ruiyi Wood Industry Company (China). Nickel nitrate hexahydrate ($Ni(NO_3)_2.6H_2O$, ACS Reagent grade), The urea was purchased from Tianjin Dingshengxin Chemical Industry Co., Ltd. High-purity CO_2 (99.999%) was purchased from Beijing Hepu Beifen Gas Industry Co., Ltd. A 0.1 M $KHCO_3$ (Sigma-Aldrich, 99.5% metals basis) solution was prepared with ultrapure water (18.2 MΩ cm) obtained from a water purification system (Hitech ECO-S15) and used as the electrolyte.

1.2 Fabrication of Ni SAs-NCW electrode

Natural basswood was cut into slices (3.5 cm×1.5 cm×2.0 mm) perpendicularly to its growth direction. The wood slices were then pre-carbonized in a muffle furnace at 260 °C for 6 h in air atmosphere and then carbonized in tube furnace at 1000 °C for 6 h with a ramping rate of 5 °C min^{-1} under N_2 atmosphere (40 mL min^{-1}). The carbonized wood (CW) slices were carefully polished with 2000 grit sand paper, washed with water, ethanol, and acetone under ultrasonication, and dried in a vacuum oven at 60 °C overnight. The CW slices were then mixed with 1 mL of concentrated nitric acid and refluxed at 120 °C for 5 h. After washing and drying, the acid-treated CW slices were immersed into a $Ni(NO_3)_2 \cdot 6H_2O$ solution (1 mg mL^{-1}) at 25 °C for 12 h to load Ni ions into the CW slices to obtain Ni^{2+}-anchored CW (Ni^{2+}-CW). The obtained Ni^{2+}-CW was further carbonized in the presence of urea as N source at 800 °C for 1 h with a ramping rate of 5 °C min^{-1} under N_2 atmosphere (40 mL min^{-1}). Afterwards, the obtained product was immersed into a HCl solution (1 M) 80 °C for 9 h to remove the Ni nanoparticles and rinsed with ultrapure water and dried in a vacuum oven at 60 °C overnight. The obtained product was termed as Ni SAs-NCW, and the sample without the HCl washing

was denoted as Ni-NCW. For comparison, NCW was synthesized using exactly the same procedure for the preparation of Ni SAs-NCW without the addition of Ni salt.

1.3 Characterization

X-ray diffraction (XRD) patterns were investigated with a Rigaku smartlab diffractometer with a nickel filtrated Cu $K\alpha$ radiation in the 2θ range of 5~80° with a scanning rate of 5° min^{-1}. Scanning electron microscopy (SEM) images were taken with a ZEISS EVO 10 scanning electron microscope. Transmission electron microscopy (TEM) images were taken with a FEI Talos F200x field emission transmission electron microscope. HAADF-STEM observations of the samples were performed on a Titan Cubed Themis G2300 STEM. X-ray photoelectron spectroscopy (XPS) measurements of the samples were performed on a ThermoFisher Escalab-250Xi electron spectrometer using an Al Kα X-ray source. Binding energies were referenced to the C 1s peak (set at 284.4 eV) of the sp^2 hybridized (C=C) carbon from the sample. The Ni content of the samples was determined by an inductively coupled plasma mass spectrometry (ICP-MS) (Agilent 7800). The specific surface areas of the samples were determined with the Brunauer-Emmett-Teller (BET) equation at 77 K by using an adsorption apparatus (Micromeritics ASAP 2460). The compression tests were carried out by a single-column system (Hz-1003) at a constant loading speed of 3 mm min^{-1}. Raman spectra were collected using a Raman spectrometer system (HORIBA Scientific LabRAM HR Evolution) using a 532 nm laser as the excitation source. The X-ray absorption spectra (XAS) including X-ray absorption near-edge structure (XANES) and extended X-ray absorption fine structure (EXAFS) of the samples were collected at the Singapore Synchrotron Light Source (SSLS) center, where a pair of channel-cut Si (111) crystals was used in the monochromator. The storage ring was working at the energy of 2.5 GeV with average electron current of below 200 mA.

1.4 Electrocatalytic CO_2 reduction reaction in a H-type cell

The electrocatalytic CO_2 reduction experiments were performed on a custom-made three-electrode system with a gas-tight H-type cell with two compartments. The cathode and anode compartments were separated with a proton exchange membrane (Nafion 117). A Pt mesh and a saturated Ag/AgCl electrode were used as counter and reference electrodes, respectively. The as-prepared self-supported electrodes were directly soldered to a Cu wire as the working electrode (1.0×1.0 cm^2). A 0.1 M KHCO$_3$ aqueous solution was used as the electrolyte. The electrochemical measurements were conducted using a CHI 660E potentiostat (CH Instruments, Inc., Shanghai, China). All of the applied potentials were recorded against Ag/AgCl (saturated KCl) reference electrode and then converted to the reversible hydrogen electrode (RHE) reference scale after iR_s compensation according to E (*vs*. RHE)=E (*vs*. Ag/AgCl)+0.0592×pH-iR_s. The solution resistance (R_s) was determined by electrochemical impedance spectroscopy (EIS) measurements, which were performed in a frequency range from 0.01 Hz to 100 kHz at a voltage amplitude of 5 mV.

The linear sweep voltammetry (LSV) was performed in the potential range of 0 to -0.8 V *vs*. RHE at a scan rate of 0.5 mV s^{-1} in N_2 or CO_2 saturated 0.1 M KHCO$_3$ solution, respectively. Prior to the experiments, CO_2 was firstly purged into the KHCO$_3$ solution for at least 30 min to remove residual air in the cathodic compartment reservoir and ensure continuous CO_2 saturation. The chronoamperometry was performed at each potential for several hours. The gas effluent from the cathodic compartment was connected to the gas sampling loop of an online pre-calibrated gas chromatography (GC, A91 Plus PANNA), which was equipped with a packed HN column and a 5 Å molecular sieve. The gas phase composition was analyzed by A91 Plus every 30 min. High purity N_2 (99.999%) was used as the carrier gas. A thermal conductivity detector

(TCD) was used to quantify H_2, while then a flame ionization detector (FID) equipped with a methanizer to quantify CO.

The Faradaic efficiency (FE) of the gas products at each applied potential were calculated by using the volume concentrations detected by the GC as below:

$$FE_i = \frac{2FV_iGtp_0}{RT_0Q_{total} \times 10^6} \times 100\%$$

where V_i (vol %) is volume concentration of CO or H_2 in the exhaust gas from the electrochemical cell (GC data) at a given sampling time, G (mL min^{-1}) is gas flow rate at room temperature and ambient pressure, t (min) is electrolysis time, p_0 is pressure (1.01×10^5 Pa), R is the gas constant (8.314 J mol^{-1} K^{-1}), T_0 is temperature (298.15 K), Q_{total} (C) is integrated charge passed during electrolysis (Chronoamperometry data), F is the Faradaic constant (96485 C mol^{-1}).

At the end of the electrolysis, the produced liquid phase products were detected by using a high-performance liquid chromatography (HPLC, Hitachi) system equipped with C18 column and UV detector. A mixture of methanol (10 %) and phosphoric acid with pH=2 was used as the mobile phase at 25 ℃ with a continuous flow rate of 0.6 mL min^{-1}.

1.5 Measurement of electrochemical active surface area (ECSA)[1]

Cyclic voltammetry (CV) tests were performed in CO_2-purged 0.05 M $K_3[Fe[(CN)_6]$. solution (0.1 M $KHCO_3$ as supporting electrolyte) to determine the electrochemical active surface areas (ECSAs) of the electrodes.

$$i_p = 2.69 \times 10^5 n^{3/2} AD^{1/2} v^{(1/2)} C$$

where i_p is the peak current value (A); n is the number of electron transfer, 2; A is the ESCA of the electrode (cm^2); D is the diffusion coefficient (cm^2 s^{-1}); C is the concentration of $K_3[Fe[(CN)_6]$ (mol cm^{-3}); v is the scanning speed (V s^{-1}).

1.6 TOF calculations[2,3]

The TOF for CO production was calculated according to the following equation:

$$TOF\ (\text{h}^{-1}) = \frac{j_{CO}/nF}{m_{cat} \times \alpha / M_{Ni}} \times 3600$$

where the j_{CO} is the partial current density for CO (A), n is the number of electrons transferred for CO, 2, F is the Faradaic constant (96485 C mol^{-1}), m_{cat} is the catalyst mass in the electrode (g), α is the Ni content in the catalysts, M_{metal} is the atomic mass of metal Ni.

1.7 Electrocatalytic CO_2 reduction in a flow cell

Self-supported Ni SAs-NCW electrode was cut into the desired size and shape and directly served as cathode in a flow cell. To increase the hydrophobicity of Ni SAs-NCW electrode, certain amount of polytetrafluoroethylene (PTFE) suspension (15 mg mL^{-1}) was spray-coated on the one side of Ni SAs-NCW electrode. A Ni foam and a saturated Ag/AgCl were used as the anode and reference electrode, respectively, which were separated by anion exchange membrane (Fumasep-FAA-3-PK-130). A 1 M KOH aqueous solution was utilized as electrolyte and pumped into cathode chamber at a flow rate of 7.5 mL min^{-1}. CO_2 was fed into cathode chamber at a flow rate of 30 mL min^{-1}.

1.8 Calculation method and modeling

All calculations were performed by density functional theory (DFT) implemented in Vienna Ab-initio Simulation Package (VASP) with Perdew-Burke-Ernzerhof function (PBE). A 5×5×1 supercell was applied in this model. The K-point mesh was 4×4×1. The spacing in the aperiodic direction is 20 Å cell to eliminate the interaction of periodic images of the system.

The free energy changes at each electrochemical step involving a proton-electron transfer were computed based on computational hydrogen electrode (CHE) model. The chemical potential of the proton-electron pairs can be calculated as a function of applied

voltage as $\mu(\text{H}^+) + \mu(e^-) = \frac{1}{2}\mu(\text{H}_{2(g)}) - eU$. The free energy of adsorbates and non-adsorbed gas-phase molecules is calculated as $G = E_{elec} + E_{ZPE} + \Delta H(0 \rightarrow T) + T\Delta S = E_{elec} + G_{(g)}$. The E_{elec} is the reaction energy of the elementary reaction obtained by DFT calculations, E_{ZPE} is the zero-point energy estimated under harmonic approximation by taking the vibrational frequencies of adsorbates or molecules as calculated within DFT. The ΔH and $T\Delta S$ are small for the adsorbates compared to E_{elec} and E_{ZPE}, and thus neglected in this study for adsorbates. The entropies of H_2 (g), CO_2 (g) and CO (g) at 1 atm are used, while the entropy of H_2O (l) is calculated at 0.035 atm, which corresponds to the vapor pressure of liquid water at 298.15 K. Due to the use of PBE functional, the non-adsorbed gas-phase CO molecule has to include a -0.51 eV correction. $G_{(T)}$ is obtained by vaspkit 1.0. The details about the energy (eV) employed in free energy Table S4 and Table S5.

2. Additional figures and tables
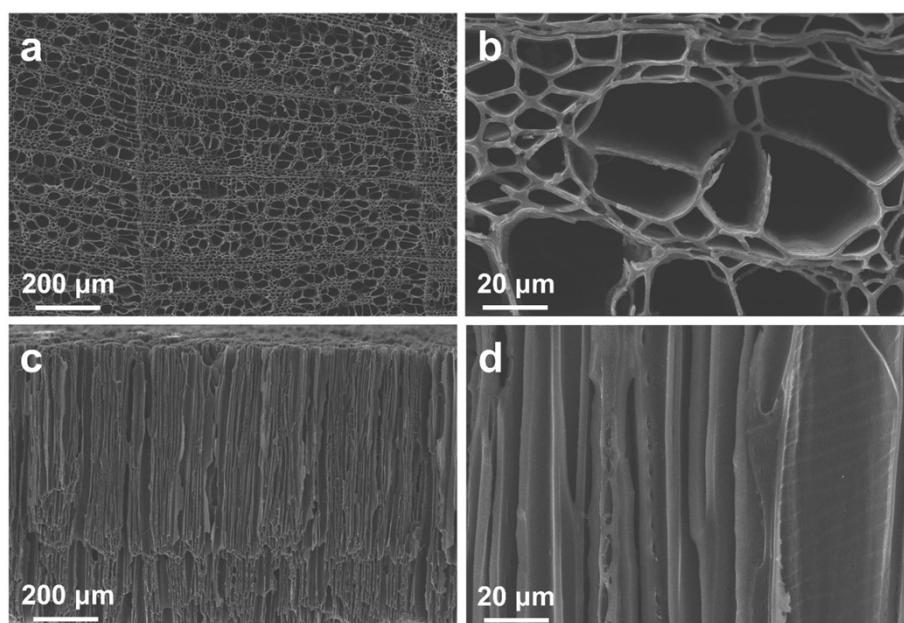
Fig. S1 (a, b) Top-view and (c, d) side-view SEM images of CW.
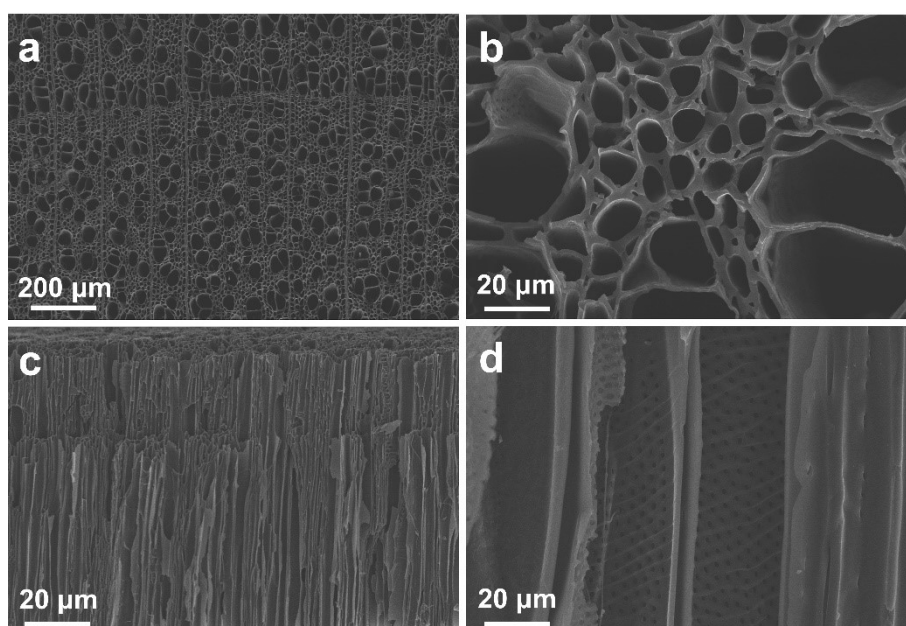
Fig. S2 (a, b) Top-view and (c, d) side-view SEM images of A-CW.
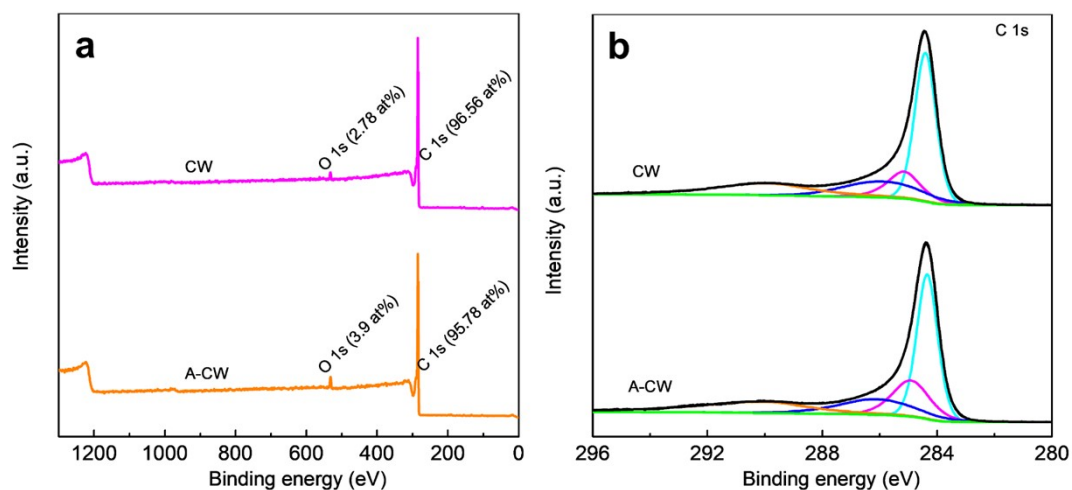
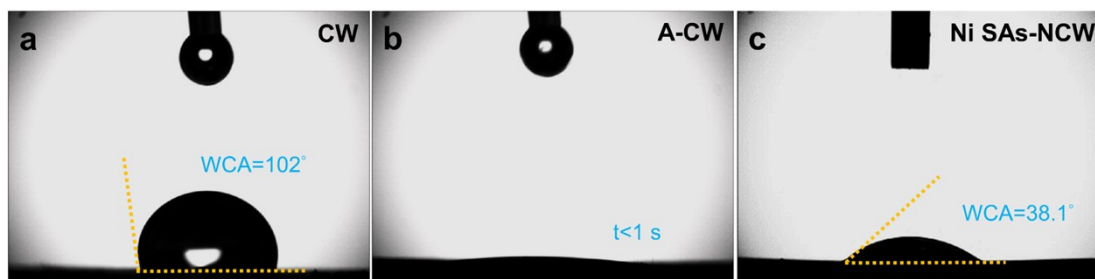**Fig. S3** (a) XPS survey of CW and A-CW. (b) XPS spectra for the C 1s region of CW and A-CW.

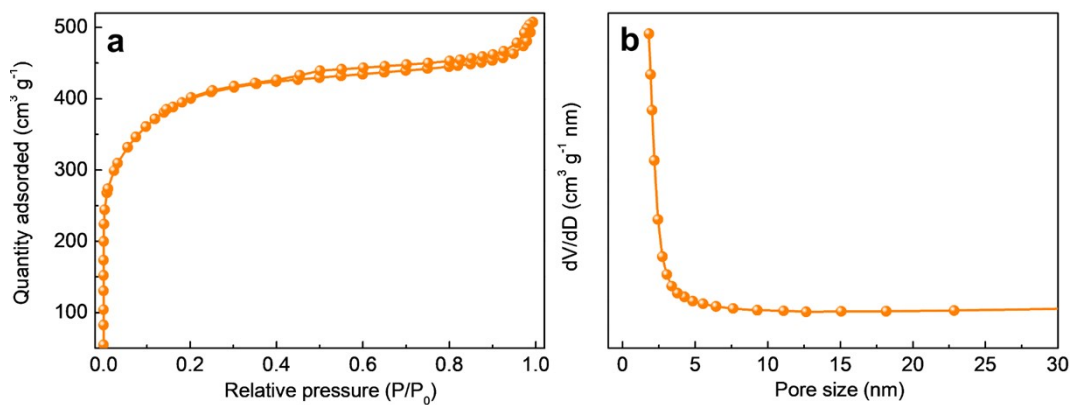**Fig. S4** Wettability of (a) CW, (b) A-CW and (c) Ni SAs-NCW.

Fig. S5 (a) N_2 adsorption-desorption isotherm and (b) the corresponding pore size distribution curve of Ni SAs-NCW.

Table S1 Textural parameters of Ni SAs-NCW electrode.

Electrode	S_{BET} (m^2 g^{-1})	Pore volume (cm^3 g^{-1})	Pore size (nm)
Ni SAs-NCW	1331.9	0.78	2.4
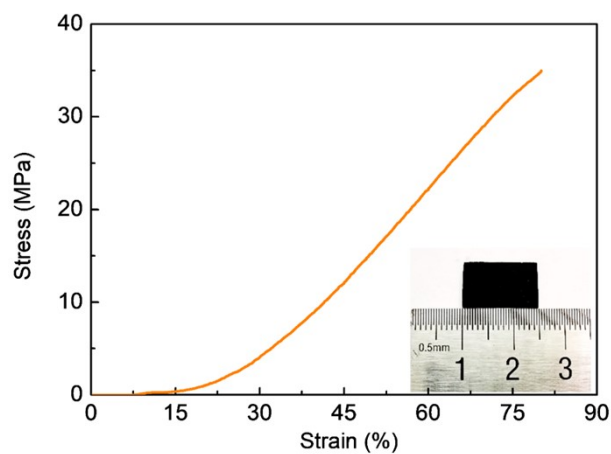
Fig. S6 Stress-strain curve of Ni SAs-NCW.
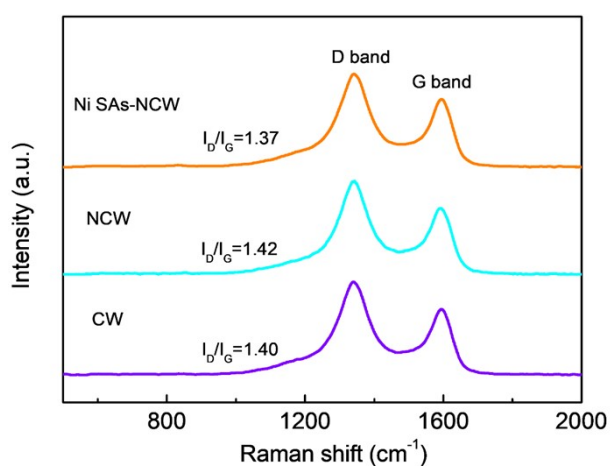
Fig. S7 Raman spectra of CW, NCW, and Ni SAs-NCW.
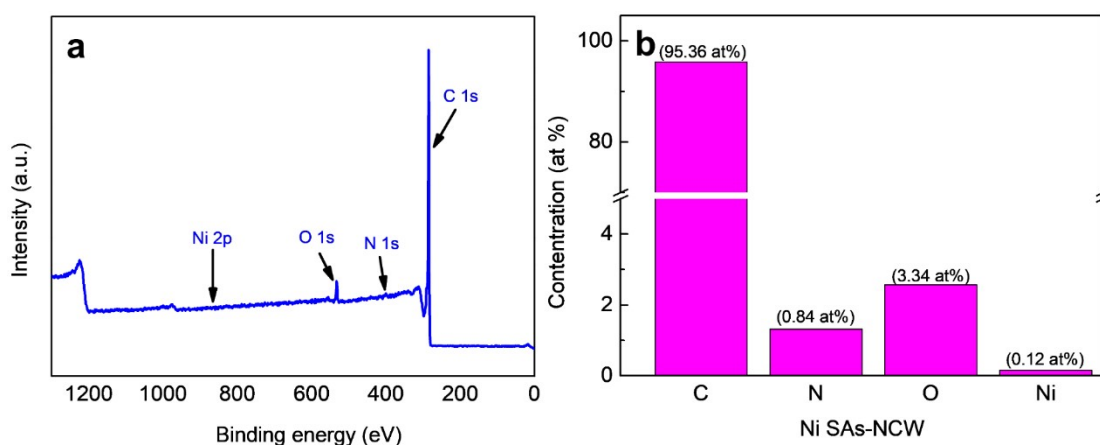
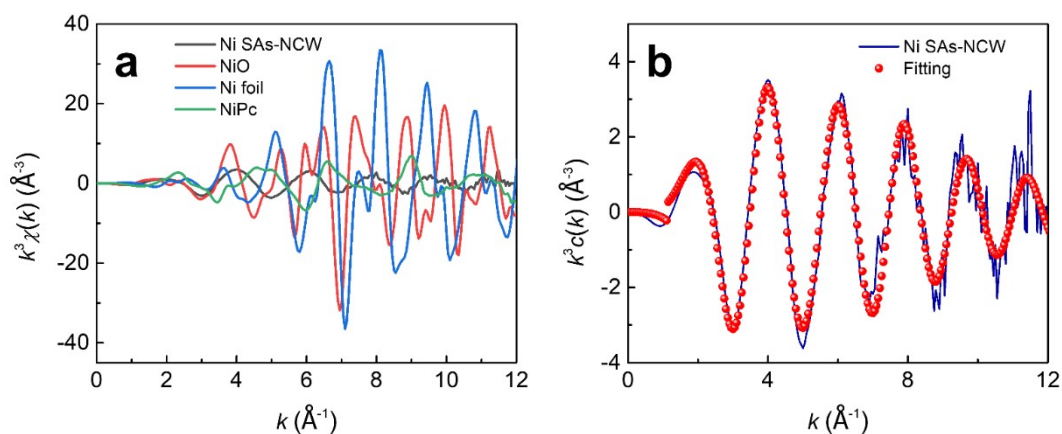**Fig. S8** (a) XPS survey spectra of Ni SAs-NCW and (b) the content of C, N, O and Ni elements.

Fig. S9 (a) The Fourier transform of EXAFS data for four samples. (b) Fitting for EXAFS data of Ni SAs-NCW.

Table S2 EXAFS fitting parameters at the Ni K-edge for various samples(S_0^2=0.838).

Sample	Shell	CN[a]	R(Å)[b]	σ^2(Å^2)[c]	ΔE_0(eV)[d]	R factor
Ni foil	Ni-Ni	12*	2.48±0.01	0.0059±0.0002	7.2±0.3	0.0015
NiPc	Ni-N	4.2±0.8	1.91±0.01	0.0045±0.0017	8.2±3.3	0.0091
NiO	Ni-O	5.6±0.8	2.07±0.01	0.0072±0.0023	-2.7±0.7	0.0083
	Ni-Ni	12.3±1.2	2.96±0.01	0.0074±0.0008		
Ni SAs-NCW	Ni-N	4.2±0.4	2.10±0.01	0.0069±0.0018	4.6±1.0	0.0087

[a] CN, coordination number; [b] R, distance between absorber and backscatter atoms; [c] σ^2, Debye-Waller factor to account for both thermal and structural disorders; [d] ΔE_0, inner potential correction; R factor indicates the goodness of the fit. S_0^2 was fixed to 0.838, according to the experimental EXAFS fit of Ni foil by fixing CN as the known crystallographic value. Fitting range: 3.0≤k (/Å) ≤14.0 and 1.0≤R (Å)≤3.0 (Ni foil and NiO); 3.0 ≤k (/Å) ≤12.0 and 1.0≤R (Å)≤2.3 (NiPc); 3.0≤k (/Å) ≤10.0 and 1.0≤R (Å)≤~2.5 (Ni SAs-NCW). A reasonable range of EXAFS fitting parameters: 0.700 <S_0^2<1.000; CN>0; σ^2 >0 Å^2; ΔE_0 <10 eV; R factor < 0.02.
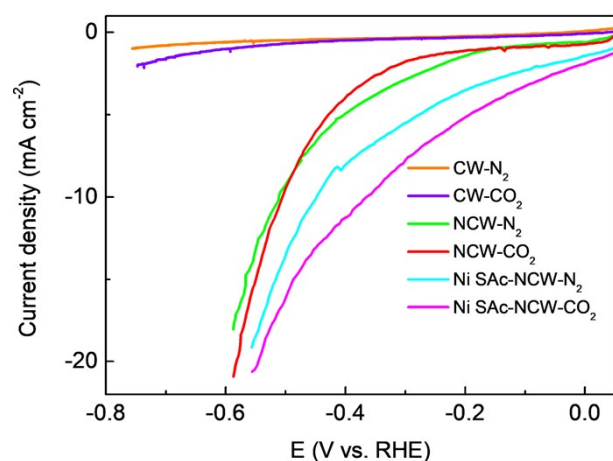
Fig. S10 LSV curves of CW, NCW, and Ni SAs-NCW recorded in N_2 and CO_2-saturated 0.1 M $KHCO_3$ aqueous solution with a scan rate of 0.5 mV s^{-1}.
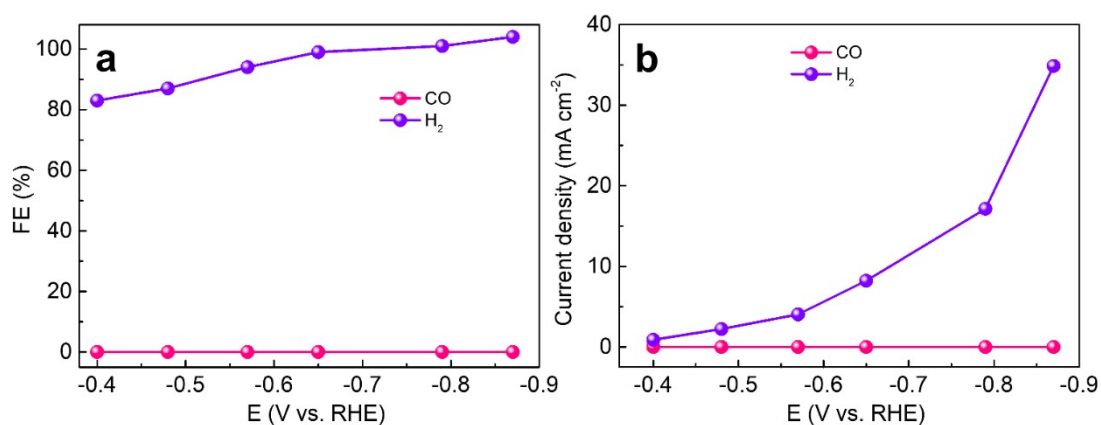

Fig. S11 FE for CO and H_2 production on Ni SAs-NCW electrode in a N_2-saturated 0.1 M $KHCO_3$ solution at various applied potentials.
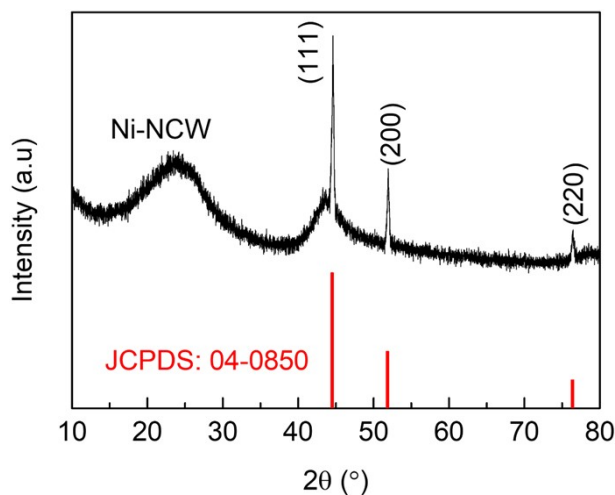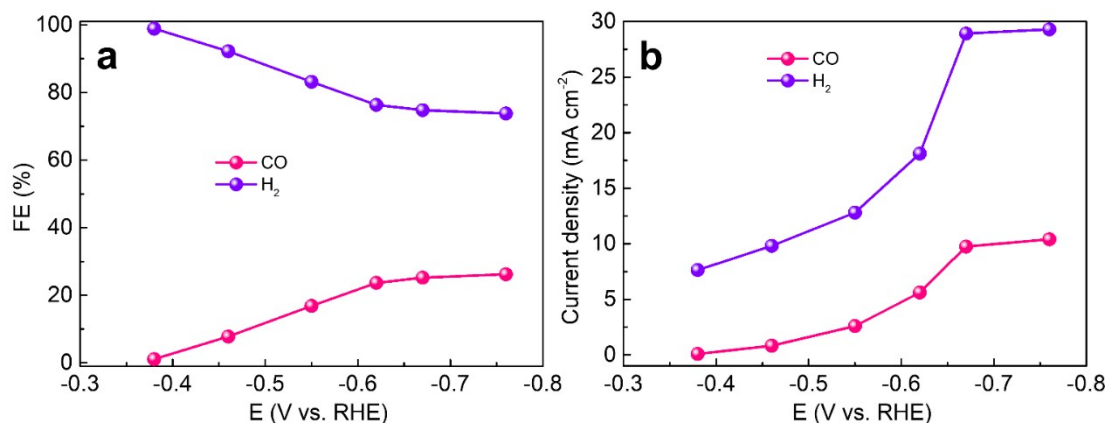

Fig. S12 XRD pattern of Ni-NCW.

Fig. S13 (a) FEs and (b) partial current densities for CO and H_2 production on Ni-NCW at various applied potentials in CO_2-saturated 0.1 M $KHCO_3$ solution.
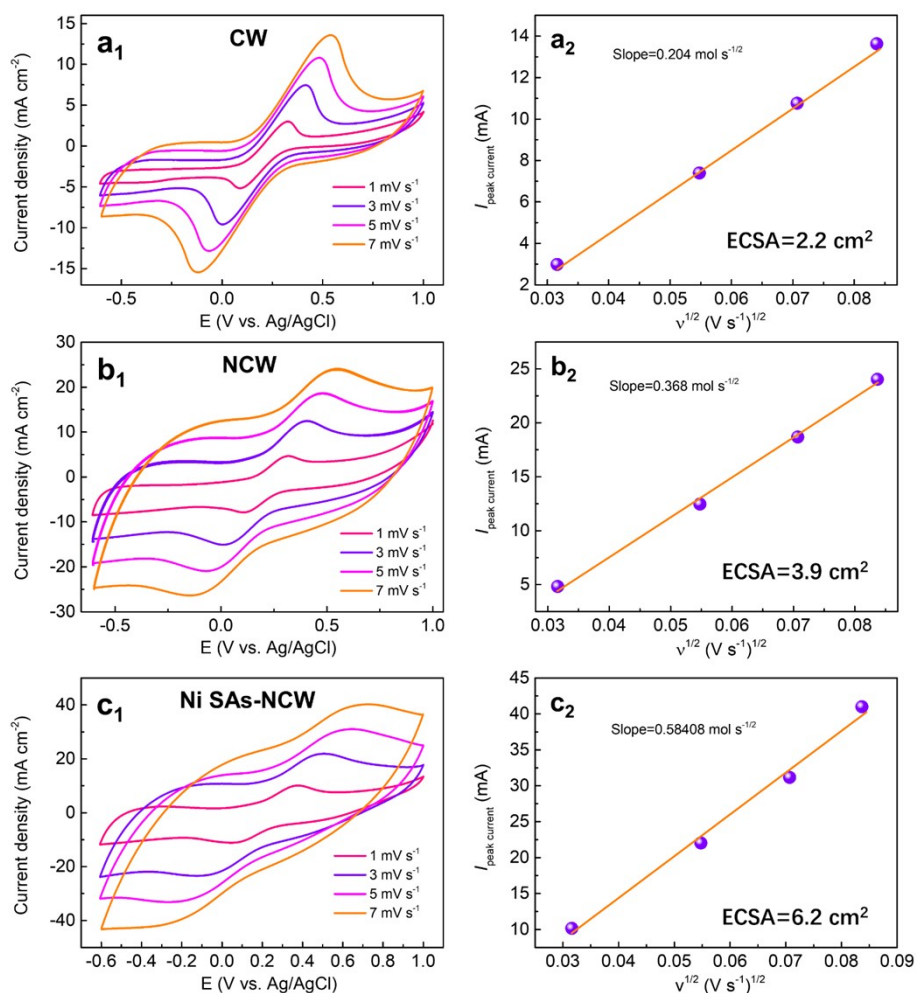

Fig. S14 CV curves and the corresponding plots of the peak current (($i_{pc}+i_{pa}$)/2) as a function of square root of the scan rate ($v^{1/2}$) measured in 0.1 M $KHCO_3$ solution containing 0.05 M $K_3[Fe[(CN)_6]$ using CW, NCW, and Ni SAs-NCW.
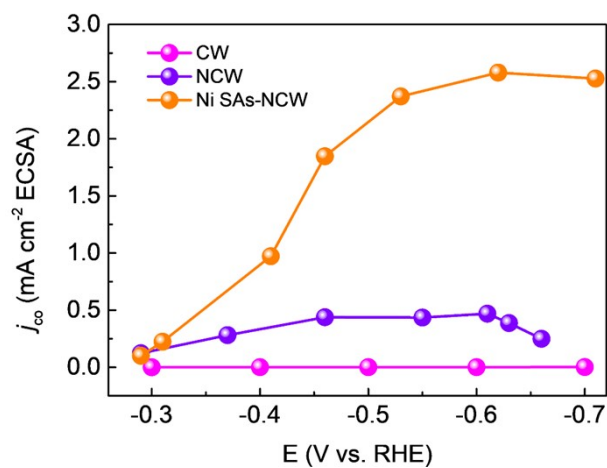
Fig. S15 ECSA-normalized partial current densities of CO production on CW, NCW, and Ni SAs-NCW.
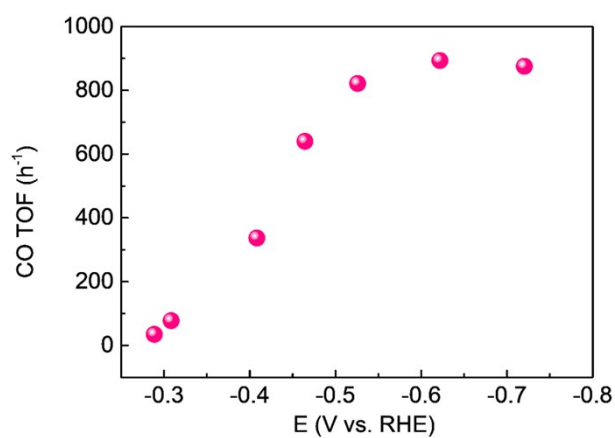

Fig. S16 TOFs of CO production per active site on Ni SAs-NCW.

Table S3 Comparison of CO_2RR performance of Ni SAs-NCW with recently reported Ni-based single-atom catalysts.

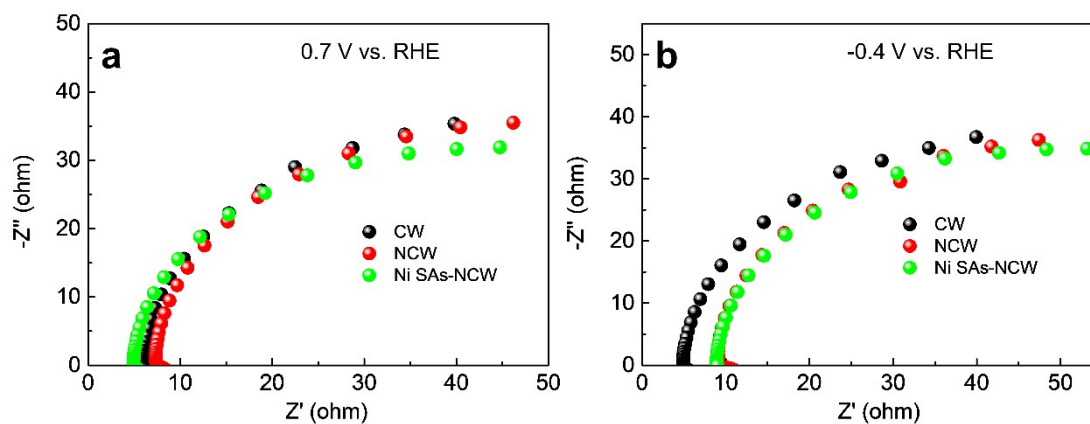| Catalyst	Electrolyte (KHCO$_3$)	E (V vs. RHE)	FEco (%)	j_{CO} (mA cm^{-2})	TOF (h^{-1})	Ref.
Ni-SAC@NC	0.5 M	-0.6	95	5.7	2400	4
Fe/Ni SAs	0.5 M	-0.7	98	7.4	~3000	5
Ni-N-CNSs	0.5 M	-0.75	95	5.5	3153.9	6
Ni SAs	0.5 M	-0.8	97	6.8	~4000	7
Ni SAs-N-C	0.5 M	-0.9	71.9	5.5	3868	8
Ni-HMCS-3-800	0.5 M	-1.0	95	10.5	15608	9
Ni-N-C	0.1 M	-0.75	97	7.51	--	10
Ni^{2+}@NG	0.5 M	-0.68	92	10.2	~2000	11
Ni@NiNCM	0.5 M	-0.9	97.6	11	--	12
SE Ni SAs@PNC	0.5 M	-0.8	94	10	--	13
Ni-Zn-N-C	0.5 M	-0.8	99	17	21851	14
NiPc/NC	0.5 M	-0.5	98	1.2	--	15
SA-NiNG-NV	0.5 M	-0.7	96	10	~1000	16
Ni SAs-NCW	**0.1 M**	**-0.46** / **-0.62**	**92.1** / **80.9**	**11.4** / **15.9**	**640** / **894**	**This work**

Fig. S17 Nyquist plots of CW, NCW, and Ni SAs-NCW in CO_2-saturated 0.1 M KHCO$_3$ solution measured at (a) 0.7 and (b) -0.4 V vs. RHE.

Table S4 The details about the energy (eV) employed in free energy.

N Species	Intermediate	E_{elec}	$G_{(T)}$	G
Pyrrolic N	COOH*	-439.81	0.62	-439.20
	CO*	-429.25	0.23	-429.02
Pyridinic N	COOH*	-473.61	0.60	-473.01
	CO*	-462.11	0.06	-462.05
Graphitic N	COOH*	-485.15	0.54	-484.61
	CO*	-476.05	0.08	-475.97
Ni-N_4	COOH*	-470.70	0.49	-470.21
	CO*	-460.31	0.02	-460.29

Table S5 Free energy (eV) corrections for species.

Species	E_{elec}	$G_{(T)}$	G
H_2	-6.77	-0.04	-6.81
CO_2	-22.96	-0.26	-23.22
H_2O	-14.22	0	-14.22
CO	-14.78	-0.39	-15.68
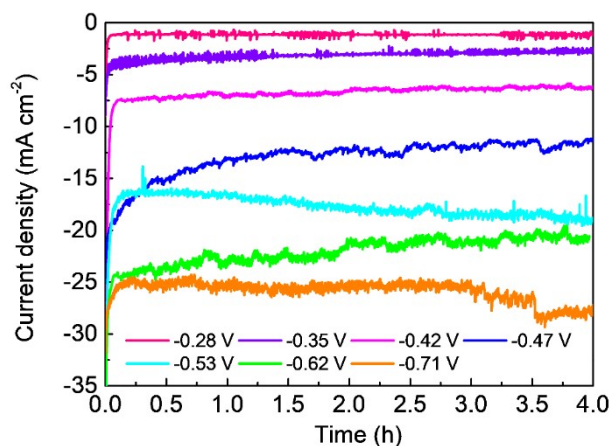
Fig. S18 Total current density of Ni SAs-NCW at different potentials in CO_2-saturated 0.1 M $KHCO_3$ solution.
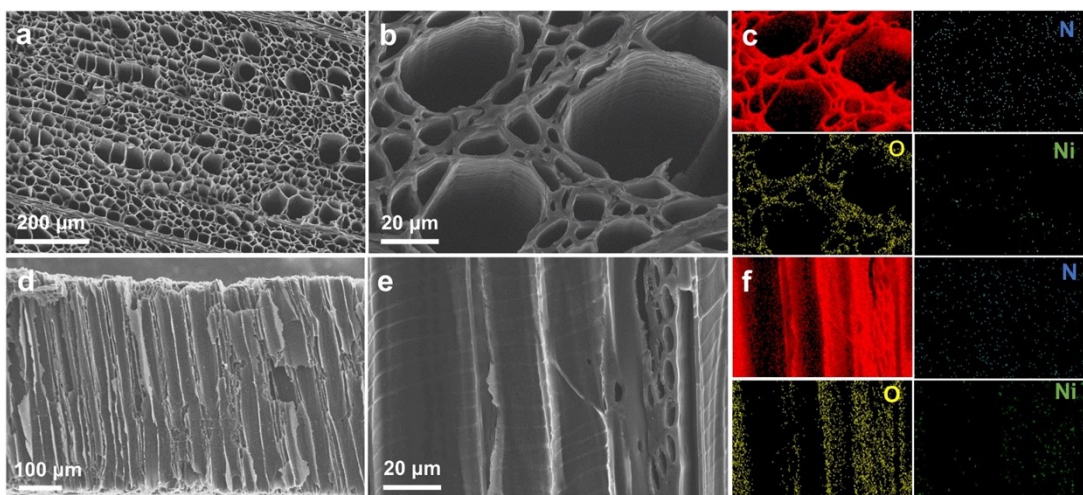
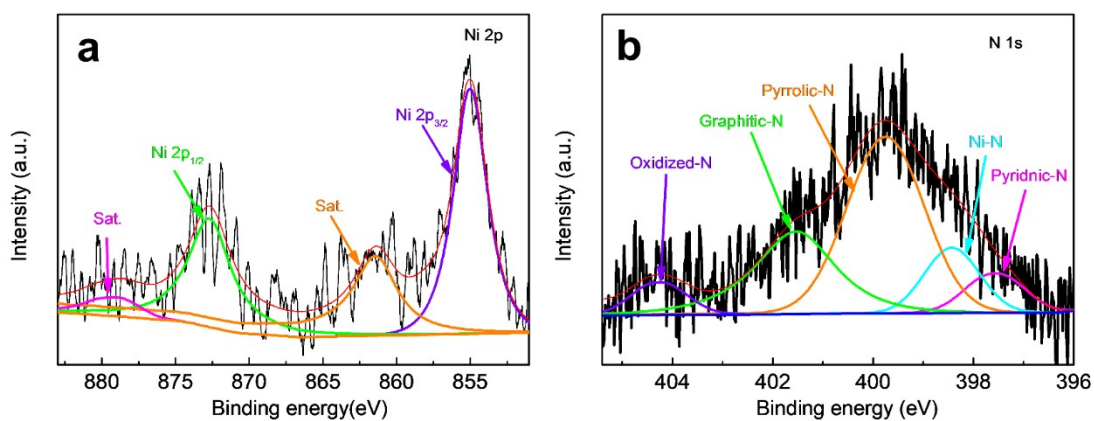**Fig. S19** SEM images of Ni SAs-NCW after CO$_2$RR and the corresponding EDX maps.

Fig. S20 High-resolution (a) Ni 2p and (b) N 1s XPS spectra of Ni SAs-NCW after CO$_2$RR.
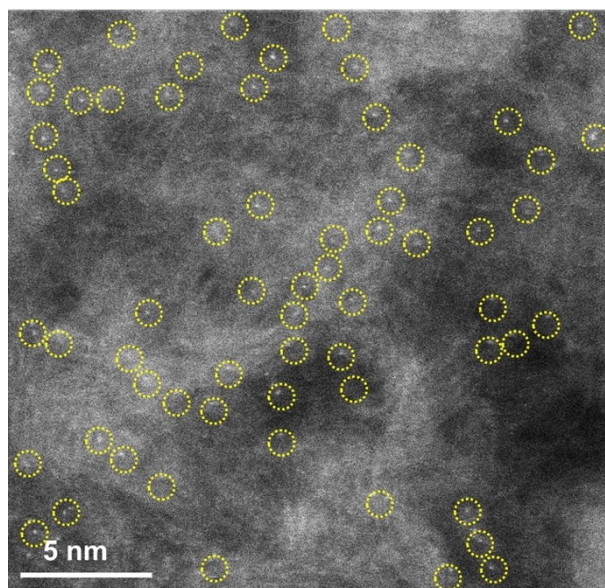
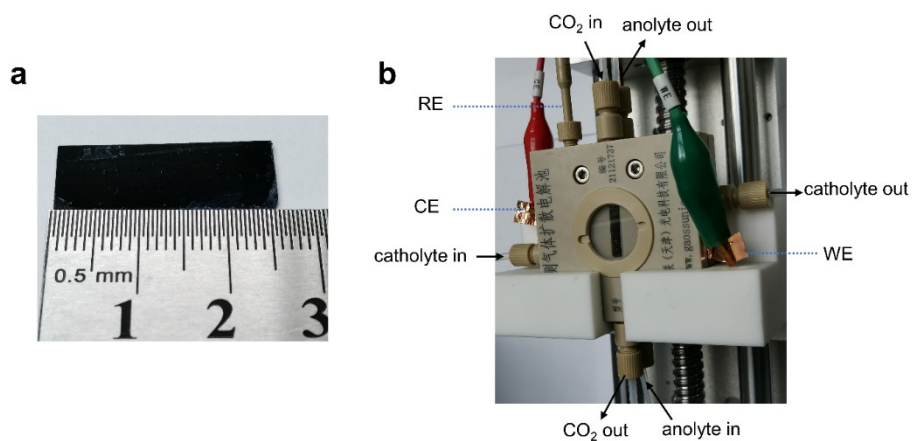**Fig. S21** Aberration-corrected HAADF-STEM image of Ni SAs-NCW after CO$_2$RR.

Fig. S22 (a) Ni SAs-NCW-based gas diffusion electrode (GDE) and (b) the photo of

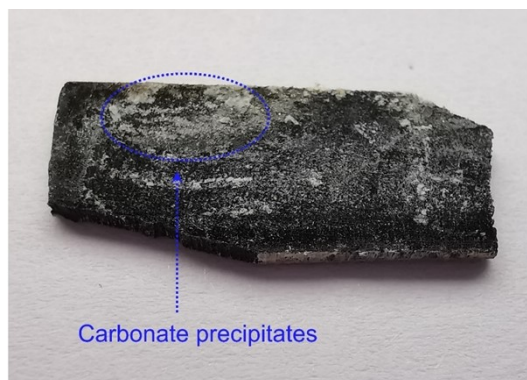the flow cell configuration for the CO$_2$RR.

Fig. S23 Photos of the back side of the Ni SAs-NCW-based GDE after stability test.

References

1. H. Pan, F. Wang, Z. G. Zhang and S. X. Min, *Sustain. Energy Fuels,* 2022, **6**, 2149-2154.

2. Z. D. Li, D. He, X. X. Yan, S. Dai, S. Younan, Z. J. Ke, X. Q. Pan, X. H. Xiao, H. J. Wu and J. Gu, *Angew. Chem. Int. Ed*., 2020, **59**, 18572-18577.

3. Y. Cheng, X. Y. Zhao, H. B. Li, S. He, J. P. Veder, J. P. Xiao, S. F. Lu, J. Pan, M. F. Chisholm, S. Z. Yang, C. Liu, J. G. Chen and S. P. Jiang, *Appl. Catal. B Environ*., 2019, **243**, 294-303.

4. Y. B. Guo, S.Yao, Y. Y. Xue, X. Hu, H. J. Cui and Z. Zhou, *Appl. Catal. B Environ.,* 2022, **304**, 120997.

5. W. Ren, X. Tan, W. Yang, C. Jia, S. Xu, K. Wang, S. C. Smith and C. Zhao, *Angew. Chem. Int. Ed*., 2019, **58**, 6972-6976.

6. Z. Ma, X. Zhang, D. Wu, X. Han, L. Zhang, H. Wang, F. Xu, Z. Gao and K. Jiang, *J. Colloid Interface Sci.,* 2020, **570**, 31-40.

7. Z. Li, D. He, X. X. Yan, S. Dai, S. Younan, Z. J. Ke, X. Q. Pan, X. H. Xiao, H. J. Wu and J. Gu, *Angew. Chem. Int. Ed.*, 2020, **59**, 18572-18577.

8. C. M. Zhao, X. Y. Dai, T. Yao, W. X. Chen, X. Q. Wang, J. Wang, J. Yang, S. Q. Wei, Y. Wu and Y. D. Li, *J. Am. Chem. Soc.,* 2017, **139**, 8078-8081.

9. W. F. Xiong, H. F. Li, H. M. Wang, J. D. Yi, H. H. You, S. Y. Zhang, Y. Hou, M. N. Gao, T. Zhang and R. Cao, *Small*, 2020, **16**, 2003943.

10. F. P. Pan, H. G. Zhang, Z. Y. Liu, D. Cullen, K. X. Liu, K. More, G. Wu, G. F. Wang and Y. Li, *J. Mater. Chem. A*, 2019, **7**, 26231-26237.

11. C. Jia, X. Tan, Y. Zhao, W. H. Ren, Y. B. Li, Z. Su, S. C. Smith and C. Zhao, *Angew. Chem. Int. Ed.,* 2021, **60**, 23342-23348.

12. W. T. Bi, X. G. Li, R. You, M. L. Chen, R. L. Yuan, W. X. Huang, X. J. Wu, W.

X. Chu, C. Z. Wu and Y. Xie, *Adv. Mater*., 2018, **30**, 1706617.

13. X. Y. Wang, X. H. Sang, C. L. Dong, S. Y. Yao, L. Shuai, J. G. Lu, B. Yang, Z. J. Li, L. C. Lei, M. Qiu, L. M. Dai and Y. Hou, *Angew. Chem. Int. Edit*., 2021, **60**,11959–11965

14. J. Yang, Z. Y. Qiu, C. M. Zhao, W. Wei, W. C. Chen, W. X. Chen, Z. J. Li, Y. T. Qu, J. C. Dong, J. Luo, Z. Y. Li and Y. Wu, *Angew. Chem. Int. Ed.,* 2018, **57**, 14095-14100.

15. X. Yng, J, Cheng, X. X. Xuan, N. Liu and J. Z. Liu, *ACS Sustain. Chem. Eng.*, 2020, **8**, 28, 10536–10543.

16. C. Jia, S. N. Li, Y. Zhao, R. K. Hocking, W. H. Ren, X. J. Chen, Z. Su, W. F. Yang, Y. Wang, S. S. Zheng, F. Pan and C. Zhao, *Adv. Funct. Mater*., 2021, **31**, 2107072.